Published in final edited form as:
Biophys Chem. 2011 February ; 154(1): 8–17. doi:10.1016/j.bpc.2010.12.001.

Partitioning of 2,6-Bis(1*H*-Benzimidazol-2-yl)pyridine Fluorophore into a Phospholipid Bilayer: Complementary Use of Fluorescence Quenching Studies and Molecular Dynamics Simulations

Alexander Kyrychenko[a,b,c,*], **Igor Yu. Sevriukov**[a], **Zoya A. Syzova**[a], **Alexey S. Ladokhin**[b,*], and **Andrey O. Doroshenko**[a,*]

[a]Institute for Chemistry, V.N. Karazin Kharkiv National University, 4 Svobody Square, Kharkiv 61077, Ukraine

[b]Department of Biochemistry and Molecular Biology, The University of Kansas Medical Center, Kansas City, Kansas 66160-7421, United States

[c]Ukrainian-American Laboratory of Computational Chemistry, Kharkiv, Ukraine and Jackson, Mississippi, United States

Abstract

Successful use of fluorescence sensing in elucidating the biophysical properties of lipid membranes requires knowledge of the distribution and location of an emitting molecule in the bilayer. We report here that 2,6-bis(1*H*-benzimidazol-2-yl)pyridine (BBP), which is almost non-fluorescent in aqueous solutions, reveals a strong emission enhancement in a hydrophobic environment of a phospholipid bilayer, making it interesting for fluorescence probing of water content in a lipid membrane. Comparing the fluorescence behavior of BBP in a wide variety of solvents with those in phospholipid vesicles, we suggest that the hydrogen bonding interactions between a BBP fluorophore and water molecules play a crucial role in the observed “light switch effect”. Therefore, the loss of water-induced fluorescence quenching inside a membrane are thought to be due to deep penetration of BBP into the hydrophobic, water-free region of a bilayer. Characterized by strong quenching by transition metal ions in solution, BBP also demonstrated significant shielding from the action of the quencher in the presence of phospholipid vesicles. We used the increase in fluorescence intensity, measured upon titration of probe molecules with lipid vesicles, to estimate the partition constant and the Gibbs free energy (ΔG) of transfer of BBP from aqueous buffer into a membrane. Partitioning BBP revealed strongly favorable ΔG, which depends only slightly on the lipid composition of a bilayer, varying in a range from -6.5 to -7.0 kcal/mol. To elucidate the binding interactions of the probe with a membrane on the molecular level, a

[*]Corresponding authors: Dr. A. Kyrychenko: Phone: (+38)-057-707-5335 alexander.v.kyrychenko@univer.kharkov.ua Prof. A. S. Ladokhin: Fax: (+1)-913-588-7440 aladokhin@kumc.edu Prof. A. O. Doroshenko: (+38)-057-707-5335 andrey.o.doroshenko@univer.kharkov.ua.

distribution and favorable location of BBP in a POPC bilayer were modeled via atomistic molecular dynamics (MD) simulations using two different approaches: (i) free, diffusion-driven partitioning of the probe molecules into a bilayer and (ii) constrained umbrella sampling of a penetration profile of the dye molecule across a bilayer. Both of these MD approaches agreed with regard to the preferred location of a BBP fluorophore within the interfacial region of a bilayer, located between the hydrocarbon acyl tails and the initial portion of the lipid headgroups. MD simulations also revealed restricted permeability of water molecules into this region of a POPC bilayer, determining the strong fluorescence enhancement observed experimentally for the membrane-partitioned form of BBP.

Keywords

Fluorescence quenching; Hydrogen boning; Excited state proton transfer; Membrane partitioning; Molecular dynamics simulations

1. INTRODUCTION

Fluorescence spectroscopy and microscopy are powerful methods to examine static and dynamics properties of lipid membranes, such as structure, ordering, hydration, fluidity and microviscosity [1,2]. The advantages of a fluorescence technique include high sensitivity and multiple measurable parameters, which enable gathering complementary information at essentially no extra experimental cost. However, to interpret these experiments, knowledge of a distribution of a fluorescent probe across a membrane and the depth of its penetration in a bilayer are essentially important [3]. Despite of a variety of spectroscopic approaches applied, these parameters have often been difficult to determine directly [4,5]. Therefore, the relationship between chemical structure and location of a fluorescent probe in a membrane has generally been difficult to define from the structure of a probe molecule [6,7]. To address these questions, molecular dynamics (MD) simulations of a distribution and location of fluorescent molecules in model membranes have become an established tool in interpreting and guiding experiments, providing a complementary microscopic view to macroscopic experimental observations [8-12].

2,6-Bis(1*H*-benzimidozole)pyridine (BBP) (Scheme 1) and its complexes with metal ions have been widely used in a variety of fluorescence applications ranging from science and engineering of new materials to biomedical researches [13-17]. The potential applications of complexes of 2,6-bis-benzimidozole-pyridines with transition metal ions in molecular photochemical devices for energy conversion have been studied extensively in the past decades [18-20]. Metal ion complexes of 2,6-bis-benzimidozole-pyridines have been reported also as fluorescent binding agents for DNA studies [21,22]. In addition, 2-benzimidozole-pyridines have revealed the high sensitivity to polarity and water contents in their local microenvironment. This is why they have often been applied for studying of solvation and hydrogen bonding dynamics on organic-water interface of micelles [23] and microemulsions [24].

In this paper, we report the fluorescence properties of BBP in phospholipid bilayers and compare them with the fluorescence behavior in water and organic solvents. We found that

BBP shows a very weak emission in neutral buffer solutions, but becomes strongly fluorescent after entering into a hydrophobic environment of a phospholipid bilayer. The changes in emission properties observed at equilibrium conditions upon titration with lipid vesicles allow us to estimate the thermodynamic parameters of partitioning, showing strong favoring for redistributing of BBP from water toward a lipid bilayer. The “light-switch” behavior of BBP in different environments can, in principle, be utilized for fluorescent probing of a water penetration depth into cell membranes. However, despite a fact that fluorescence measurements can provide thermodynamic information, such as a partition coefficient and the Gibbs free energy of the water-to-bilayer transfer, a spatial distribution of BBP across a lipid bilayer remains unknown. Therefore, we complemented the experimental fluorescence measurements with atomistic molecular dynamics (MD) simulations to study various kinetic and thermodynamics processes governing binding and the transfer of BBP into a model lipid bilayer. Here we applied our recently developed method, allowing for a joint refinement of the probe distribution and location in a model membrane using fluorescence measurements and MD simulations [25-27]. To take into account a bulk character of a BBP fluorophore, the MD approach for computing a penetration profile of a probe across a bilayer is now improved by using constrained sampling of two probe molecules at a time. While a good agreement between the thermodynamic parameters of partitioning provided with these two, experimental and computational, methods can prove the validity of the approach applied, it can be in turn utilized for testing and improving the reliability of the MD model and force-filed parameters.

2. EXPERIMENTAL AND COMPUTATIONAL SETUP

2.1 Materials

The synthesis and purification of 2,6-bis(1H-benzimidazol-2-yl)pyridine have been described elsewhere [28,29]. 1-Palmitoyl-2-oleoyl-*sn*-glycero-3-phosphatidylcholine (POPC), 1-palmitoyl-2-oleoyl-*sn*-glycero-3-phosphatidylglycerol (POPG), and cholesterol (Chol) were obtained from Avanti Polar Lipids (Alabaster, AL). Large unilamellar vesicles (LUV) of 0.1 μm diameter were prepared by extrusion as previously described [30,31] using the following molar mixtures of POPC and POPG: 1:3 (25POPC/75POPG) and 3:1 (75POPC/25POPG). Lipid concentrations of stock solutions were determined according to the procedure of Bartlett [32].

2.2 Fluorescence measurements

Fluorescence was measured using either Hitachi F4010 or SPEX Fluorolog FL3-22 (Jobin Yvon, Edison, NJ) steady-state fluorescence spectrometer. The latter was equipped with double-grating excitation and emission monochromators. The measurements were made in a 2 × 10 mm cuvette oriented perpendicular to the excitation beam and maintained at 25 °C using a Peltier device from Quantum Northwest (Spokane, WA). Quinine bisulfate in 0.1 N H_2SO_4 (ϕ_f=0.546) was used as the reference standard for measurement of the fluorescence quantum yield [33].

The apparent partition coefficient K_p was calculated by fitting fluorescence intensities, $I_i$measured at fixed wavelength to equation [Eq. (1)]:

$$I_i([L]) = I_0 + (I_{max} - I_0)\frac{K_p[L]}{[W] + K_p[L]} \quad \text{(Eq. 1)}$$

in which the fluorescence intensities I_0 = the initial fluorescence signal in water in the absence of LUV; fluorescence intensities I_{max} = the maximal fluorescence increase on the complete partition, [L] = the molar concentration of lipid, [W] = the molar concentration of water (55.3 M), K_p = the mole fraction partition coefficient [34]. The Gibbs free energy ΔG of transfer from water to a lipid membrane was estimated from the mole fraction coefficient K_p using equation [Eq. (2)]:

$$\Delta G = -RT \quad ln \quad K_p \quad \text{(Eq. 2)}$$

2.3 MD simulation setup

We modelled a phospholipid bilayer consisted of 128 lipid molecules of 1-palmitoyl-2-oleoyl-*sn*-glycero-3-phosphatidyl-choline (POPC) (64 per leaflet) and hydrated by 4553 water molecules. The equilibrated configuration of a POPC bilayer was taken from our previous work [25]. A MD force field of a POPC bilayer was adopted from reference [35] in which CH_2 and CH_3 groups of a POPC molecule were treated as united atoms. The Simple Point Charge (SPC) model [36] was used for water. The bond length and angles parameters for BBP were optimized by density functional theory calculations at the B3LYP/cc-pVDZ level and adopted for the format of GROMACS force field. Dihedral angle rotation around the C-C bond, connecting the benzimidazole and pyridine rings, was modeled using the periodic Ryckaert-Bellemans dihedral potential [37]. Partial charges needed for Coulomb interactions were derived from the B3LYP/cc-pVDZ optimized electron densities by fitting the electrostatic potential to point (ESP) charges. The reliability of the force field for BBP was tested as described previously [38]. The detailed force field parameters for BBP are given in Supplementary Material.

All MD simulations were carried out at the constant number of particles, constant pressure, P = 1 atm, and the constant temperature, T = 298 K (NPT ensemble). Three-dimensional periodic boundary conditions were applied with the z axis lying along a direction normal to the bilayer. The pressure was controlled semi-isotropically, so that the *x*-*y* and *z* dimensions of the simulation box were allowed to fluctuate independently from each other, keeping the total pressure constant. The reference temperature and pressure were kept constant using the Berendsen weak coupling scheme [39] with coupling constant of τ_T=0.1 ps for the temperature coupling and $\tau_{P(x\text{-}y)} = \tau_{P(z)}$=1.0 ps for the pressure coupling. The cutoff distance of Lennard-Jones and Coulombs interactions was equal to 1.4 nm. The long-range Coulombs interactions were accounted for using the Particle Mesh Ewald (PME) approach [40]. All bond lengths in POPC and BBP were kept constant using the LINCS routine [41]. The MD integration time step was 2 fs.

A formalism of the potential of mean force was used to calculate a free energy profile of probe penetration across a bilayer. To calculate the free energy of transfer of a probe across the bilayer normal (the direction of the *z* axis), we define the reaction coordinate by the *z*

axis and accumulate the z-component of the force acting on the molecule F_z at a certain constrained distance d_c between the probe and the bilayer center of mass at different positions z along the reaction coordinate. A harmonic restraint of 1500 kJ mol^{-1} nm^{-2} was applied to distance d_c between the center of mass of the pyridine ring of a probe molecule and the center of mass of a POPC bilayer. This procedure gives the free energy for the transfer process between points z_1 and z_2 as [Eq. (3)]:

$$\Delta G = \Delta G_{z2} - \Delta G_{z1} = -\int_{z1}^{z2} \langle F_z \rangle_z d_z \quad \text{(Eq. 3)}$$

where the bracket F_z means that the force are averaged at a certain constrained point z of the reaction path. The potential of mean force was calculated from the biased distributions using the weighted histogram analysis method [42]. A total of 33 restraint points were sampled in the direction normal to the bilayer. For each restraint points, the system was first equilibrated at an elevated temperature of 323 K for 1 ns, after which the actual MD sampling was run at 298 K for 2 ns. The MD simulations were carried out using GROMACS set of programs, version 4.0.5 [43]. Molecular graphics and visualization were performed using VMD 1.8.6 software package [44].

3. RESULTS AND DISCUSSION

3.1 Fluorescence Behavior in Organic Solvents and in Aqueous Solution

The electronic absorption and fluorescence spectra of BBP in organic solvents have been reported elsewhere [14-16,20]. Here, we briefly summarize these photophysical properties (Table 1) and examine the fluorescence behavior of BBP in 50 mM sodium phosphate buffer at pH 8 in the presence and in the absence of LUVs. As seen from Table 1, the photophysical properties of BBP are characterized with high quantum yield fluorescence in both nonpolar and polar organic solvents. However, strong fluorescence quenching, manifested itself as a decrease in the fluorescence quantum yield (ϕ_{fl}), was observed in aqueous solutions (Table 1). Upon passing from toluene to phosphate buffer at pH 8, ϕ_{fl} was decreased by a factor of 74 changing from 0.37 to 0.005 (Table 1).

It is interesting that titration of buffer solution of BBP with lipid vesicles leads to a strong enhancement of fluorescence. Examples of typical changes in emission spectra of BBP in aqueous buffer as a function of LUV concentration are shown in Figure 1. In aqueous buffer, the emission spectrum of BBP had λ_{max}=395 nm when excited at 315 nm. In addition, the fluorescence enhancement upon LUV titration was also accompanied with a blue shift of λ_{max} which reaches value of 379 nm at the complete partition (Table 1). These spectral changes of BBP are indicative of partitioning of a fluorophore into LUV, when it leaves polar aqueous solution and enters a nonpolar hydrophobic environment inside a lipid vesicle.

3.2 Thermodynamics of Partitioning into a Lipid Bilayer

To estimate the mole fraction partition coefficient K_p for transfer of BBP from aqueous buffer solution into a vesicle, we used the increase in fluorescence intensities measured at 379 nm. Figure 2 illustrates how the experimental titration plots of BBP vary depending on the composition of LUVs, changing from pure POPC to 75:25 and 25:75 molar ratios of POPC/POPG, respectively. The solid curves show least squares fits of Eq. 1 (see

Experimental Section) to these data giving relevant fitting parameters, such as the fluorescence increase on the complete partition I_{max} and partition coefficient K_p. The partition free energy ΔG of the transfer was calculated using Eq. 2 and summarized in Table 2.

Figure 2 and Table 2 show that the fluorescence signal of BBP, observed upon the complete partition (I_{max}), varies significantly, starting from 8.5-fold increase upon partitioning to LUV composed of 25POPC/75POPG and ending to ~62-fold increase in the case of partitioning to pure POPC LUV. In addition, the presence of 10% of cholesterol in POPC LUV results in a decrease in I_{max} of a factor 3.7. The results shown in Figure 2 demonstrate that the magnitude of I_{max} decreases as the mole fraction of anionic POPG lipids in LUV and, hence, the negative surface potential of a model membrane increases. There are two possible scenarios explaining the lipid-dependent fluorescence behavior of BBP: According to the first scenario, the increase in the fraction of POPG lipids in LUV may lead to an overall decrease in binding and the partitioning affinity of BBP for negatively charged LUVs. In the second scenario, the complete partitioning of BBP into anionic 25POPC/75POPG LUV may still occur; however, partitioned probe molecules are located in an interfacial region of LUV, in which they become more accessible to quenching with water molecules. The latter scenario is consistent with observation that the significant decrease in I_{max}, which is observed upon going from pure POPC to 25POPC/75POPG LUVs, is accompanied with only a moderate decrease in ΔG changing from - 7.0 to -6.5 kcal/mol (Table 2).

3.3 The Origin of Fluorescence Quenching in Water

No new emitting species was detected for BBP in water, but the fluorescence quantum yield decreased dramatically, indicating the appearance of a fast $S_1 \rightarrow S_0$ nonradiative channel. It has been established that emission of a fluorophore is often strongly quenched in bulk water due to formation of an intermolecular hydrogen bond [45-49]. Quite often, intermolecular H-bonds provide an efficient channel for radiationless dissipation of an excessive energy of electronically excited molecules, as a result of an overall increase in the rate of internal conversion [50-52]. In terms of hydrogen bonding with protic partners, BBP is bifunctional acting simultaneously as a H-bond donor and as an acceptor (Scheme 2, form I).

The structure of BBP also suggests that it can exist in several conformations, each of which is capable of forming various types of hydrogen-bonded complexes with water molecules, attached either to the NH groups or to the pyridine nitrogen (Scheme 2). Experimental and theoretical developments have demonstrated that water-induced fluorescence quenching might be activated by an excited state proton transfer (ESPT) reaction, occurring along an intermolecular hydrogen bond [45,51,52-54]. However, in such a bifunctionally hydrogen bond forming fluorophore as BBP, a new photophysical feature may appear. If geometrical criteria are favourable, the donor and acceptor moieties may form a hydrogen bond intramolecularly, opening up the possibility for a direct ESPT reaction, occurring from the benzimidazole NH group toward the pyridine atom, as shown in Scheme 2 for form II. If it is not the case, ESPT can still occur along a cyclic hydrogen-bonded bridge formed by a water molecule, as shown in Scheme 2 for form III.

A limited number of examples exists demonstrating that direct ESPT could indeed be observed in chromophores, in which a weak intramolecular H-bond of a N-H···N type may be formed in a quasi-five-membered ring, composed of 2-pyridyl ring substituted with either pyrazole [55] or pyrrole [56,57]. On the other hand, there have been numerous observations when ESPT could proceed via proton migration along hydrogen-bonded bridges consisting of water [45,58-60], alcohol [45,61-62], or ammonia [63-64]. One of the best known systems, possessing a similar donor-acceptor topology, is a family of structurally related 2-pyridylindoles, which H-bond-controlled excited state behavior has attracted considerable attention [65-69]. Recent developments in *ab initio* computational modeling have suggested that the electronic excitation of H-bonded pyridine-pyrrole moieties may lead to a strong correlation between electron- and proton transfer processes, so that hydrogen-bonding-induced phenomena in these systems can be described in terms of the electron-driven-proton-transfer mechanism proposed by Sobolewski and Domcke [70,71]. Finally, an alternative mechanism of fluorescence quenching by hydroxylic solvents, involving excited state protonation of the pyridine nitrogen atom, which is followed by twisting of the pyridyl moiety has recently been proposed by Waluk and coworkers [72].

From the foregoing discussion it appears that the photophysical behavior of BBP in water might be rather complicated, involving all the above mechanisms. Leaving aside the detailed elucidation of the quenching origin, it seems to be evident that specific H-bonding with water molecules plays a crucial role in the strong fluorescence quenching of BBP in a bulk aqueous environment. The purpose of the present work is to show that the fluorescence enhancement of BBP observed upon LUV partitioning is indicative of the loss of these specific hydrogen bonding interactions in a hydrophobic membrane environment.

3.4 Fluorescence Quenching by Co^{+} Ions

Quenching of fluorescence of a probe molecule with transition metal ions is one of the well-established ways to obtain information about a partition depth of membrane-bound fluorophores [73,74]. Collisional quenching in solution can be described by the classic Stern-Vollmer equation [Eq. (4)]:

$$\frac{F_0}{F_i} = 1 + K_{SV}[Q] \quad \text{(Eq. 4)}$$

where, F_0 and F_i are the fluorescence intensities in the absence and the presence of quencher, respectively; [Q] = the concentration of the quencher; K_{sv} = the Stern-Vollmer quenching constant.

Figure 3 shows results of fluorescence quenching BBP by Co^{2+} ions in aqueous buffer solution and when partitioned into LUV, together with the fitted Stern-Vollmer plots. The good linearity of Stern-Vollmer dependencies indicates that only one type of quenched fluorophores is present and, therefore, the simple analytical form of Stern-Vollmer equation [Eq. (4)] can be applied. As it can be seen, fluorescence of free BBP in aqueous solution is strongly quenched by Co^{2+} ions. However, in the presence of LUV much less quenching occurs. For unbound BBP in aqueous buffer, K_{sv} is found to be 42×10^5 M^{-1}. In the presence of pure POPC, 90POPC/10Chol, and 25POPC/75POPG LUVs K_{sv} is decreased to 0.8×10^5,

1.1×10^5, and 1.4×10^5 M^{-1}, respectively. The strong decrease of K_{sv} points to the fact that BBP after its partitioning into LUV becomes almost inaccessible to the quencher. It is important to note that the extent of the quenching depends insignificantly on the composition of LUV. Comparing the Co^{2+} quenching data with the LUV titration plots shown in Figure 2, we can conclude that despite of the relatively weak increase in fluorescence observed upon the membrane partitioning, BBP can still be efficiently shielded by 90POPC/10Chol and 25POPC/75POPG LUVs from quenching by Co^{2+} ions.

3.5 MD Simulation of BBP in a POPC Bilayer

Molecular dynamics simulations can provide detailed atomistic descriptions of studied systems, and it can be applied as a complementary method, clarifying the above series of the fluorescence quenching experiments. Indeed, there are a lot of convincing examples of complementary uses of experimental spectroscopy studies and MD simulations, in which combining of the above methods led to better understanding of the mechanism of the interactions of small molecules with lipid membranes [8-10,12,75]. Here we applied atomistic MD simulations to examine the distribution and favourable location of BBP in a POPC bilayer using two different approaches; the first approach was based on MD simulations of passive, diffusion-driven partitioning of several molecules of BBP from bulk water into a bilayer. In the second approach, MD umbrella sampling of the potential of mean force (PMF) was utilized for calculation of a free energy profile of penetration of BBP across a bilayer. These two approaches have been widely used to provide mechanistic insights into structural aspects and energetics of interactions of solutes and ions with a membrane [25,26,76-79], both having certain advantages and limitations. The method of conventional, unbiased simulations of the passive partitioning is believed to reproduce actual experimental conditions of a free choice of a probe for its own modes of interactions with lipid membranes. Moreover, to improve MD sampling statistics, the binding interactions of several probe molecules with a membrane may be simulated simultaneously [8,25-27,80]. This approach however is still computational demanding. Depending on sampling times, a final probe distribution may converge very slowly and, therefore, it may be dependent on the choice of an initial configuration of a MD system. On the other hand, biased PMF calculations, which are rather limited in reproducing equilibrium properties, they however have an advantage of better sampling of thermodynamically unfavorable regions of the probe-bilayer system [11,25,77-79].

3.5.1 Passive Distributing of BBP between Water and a Bilayer—Firstly, we applied the method of the passive diffusion to examine the binding interactions of BBP with a POPC bilayer. To elucidate the role of starting configurations in predicting the equilibrium distribution of a probe within a membrane, four BBP molecules were placed in different positions and in random orientations into the bulk water phase in close proximity to surface of a POPC bilayer, two molecules on the top and at the bottom leaflets. The starting configuration of the system at t=0 ns is shown in Figure 4(top). Although the four BBP molecules were initially placed at different positions in the vicinity of the bilayer, we observed that, during the first 30 ns period, all of them migrated into the headgroups region inside the lipid bilayer, Figure 4(middle). We would like to note that when the molecules

reached the above discussed region, no further systematic movement deeper along the bilayer normal was observed during an additional 40 ns of the sampling [Figure 4(bottom)].

To trace the movement of each probe molecules the positions of their center of mass (COM) were plotted along the bilayer normal axis Z as a function of the simulation time, Figure 5. As can be seen from Figure 5, all the probe molecules moved rapidly toward the bilayer surface during the first 10 ns, after which their COMs movement reaches some plateau. An almost symmetric Gaussian-type distribution centered around 16 Å from the bilayer midpoint was produced by averaging the COM trajectories along the bilayer normal *Z* for the last 50-ns sampling period (not shown). This distribution corresponds to the average residence position of BBP in a POPC bilayer. Taking into account the distribution broadening width, we found that BBP prefers to locate in the region around 16±3 Å from the bilayer midpoint. It is interesting that, during the whole 70 ns sampling period, there was no trend for the BBP molecules to move from one monolayer leaflet of the bilayer across the hydrophobic core to the other half.

3.5.2 Umbrella Sampling of Penetration across a Bilayer—To evaluate the Gibbs free energy profile of BBP penetration across a POPC bilayer, we used the method of the potential of mean forces [42] based on a series of constrained MD samplings. Figure 6 shows the umbrella sampling scheme used for computing the PMF. To gather additional statistics, two BBP molecules were sampled simultaneously, so that when the first molecule reaches the center of a bilayer, the second molecule appears in the bulk water (Figure 6).

We carried out a series of MD runs, in which the center of mass of the pyridine moiety of BBP was restrained with respect to the center of mass of the POPC bilayer at distance d_c. At the same time, despite of the restraining of the center of mass of the pyridine ring, rotation of the whole molecule was still allowed. To construct the PMF, distance d_c was varied starting from 35 Å (bulk water) to 0 Å (the center of the bilayer). Figure 7 shows the PMF of a penetration profile of BBP across a POPC bilayer. We treated the each of the two BBP probes as two independent samples, which allow us to estimate sampling errors. In the limit of infinite sampling, the PMF errors should be close to zero; however, as can be noticed from Figure 7, depending on positions in a bilayer, the estimated sampling errors were found to be as large as 1.5 kcal/mol.

The PMF profile for BBP shows a favorable free-energy well of -8.1 kcal/mol centered around 15 Å from the center of a bilayer, Figure 7. The profile suggests that BBP enters the bilayer with no essential free energy costs; however, as BBP approaches the minimum of the free energy well, it experiences a large (4.3 kcal/mol) barrier to reach the center of the bilayer. Interestingly, the PMF profile agrees well with the preferred localization of BBP in a POPC bilayer estimated with the unbiased passive partitioning. Both passive and constrained MD approaches provide evidences that BBP favors residence in a region of the bilayer at around 15-16 Å from the center. Moreover, the Gibbs free energy of the bilayer penetration calculated with the PMF shows the overall agreement with the experimental ΔG of the membrane partitioning detected experimentally using fluorescence titration by LUV (Table 2).

3.5.3 Depth-Dependent Probability of Probe−Water H-Bonding in a Bilayer— Taking into account that the water-induced fluorescence quenching is expected to be dependent on a penetration depth of BBP inside a bilayer, we therefore estimated the probability of probe–water hydrogen-bonding across the POPC bilayer. As can be seen from Scheme 2, BBP could form various H-bonded complexes with water. Therefore, we focused our attention on the formation of the H-bond between the N-H groups of the two benzimidazole moieties of BBP and an oxygen atom of water molecules. We first defined geometric criteria for the formation of the discussed hydrogen bond, as shown schematically in Figure 8A. The occurrence of the probe– water hydrogen bond was established when two geometric criteria (distance and angle) were valid: (1) the distance r_i between the nitrogen atom of the NH group and the oxygen atom of water is $r_i \leq r_{HB} = 3.5$ Å; (2) the angle made by the N-H atoms and the water oxygen is $\alpha_i \leq \alpha_{HB} = 0° \pm 30°$. The total number of the H-bonds per a BBP molecule was estimated for each 100 ps time frame over the whole period of the MD sampling, during which BBP was restrained at the certain distance dc along the bilayer (see Figure 6 for more details). Since this procedure monitors the formation of the H-bond with the two benzimidazole NH groups, the probability of BBP–water H-bonding therefore was defined as a half of the average number of the H-bonds counted in the whole sampling period.

Figures 8B and 8C show a plot of the BBP–water H-bonding probability as a function of its penetration depth across a POPC bilayer. When BBP moves from the bulk water and enters the bilayer the H-bonding probability decreases sharply. When BBP moves farther inside the bilayer in the region of the hydrophobic core, the probability falls to the values below 10%. Figure 8C superimposes the BBP–water H-bonding probability on the profiles of mass densities, averaged for the whole POPC bilayer and all water molecules. The latter profile corresponds to a permeation profile of water inside the POPC bilayer. Such water behavior is in agreement with the limited permeation of interfacial water molecules into the different regions of lipid bilayers reported by Berkowitz and Jungwirth [81,82]. As it can be noted from Figure 8C, there is a correlation between water-to-bilayer permeability and the probability for BBP–water H-bonding. It is also interesting that when the water permeability profile falls to zero in the middle of the bilayer, some residual probability of BBP–water H-bonding still remains, indicating the incomplete loss of the water solvation shell by the probe.

3.5.4 Membrane Perturbations and Water Defects—As it has been reported earlier [83] the biased penetration of large aromatic compounds into a lipid membrane could lead to the perturbation of the bilayer structure. Numerous computational studies were reported that partitioning of polar or charged molecules (drugs, amino acid residues, etc) into the hydrocarbon core was often accompanied with the formation of large water defects across interface of a bilayer [84-86]. Therefore, special care was taken to insure that the umbrella sampling simulation of bulk-sized BBP in a POPC bilayer was accompanied with no significant membrane perturbations.

When BBP entered from the water phase into the bilayer, the formation of definite water defects on the bilayer surface was observed. These defects were formed mainly once the bulk core of BBP was placed at distances 10-13 Å from the bilayer center. The formation of

the water defects was strongly dependent on a rate of BBP migration from the water phase inside the bilayer. We observed that if BBP was rapidly transferred into the bilayer, the water solvation shell molecules surrounding the BBP fluorophore could penetrate deeply into the hydrophobic region of the bilayer. Therefore, pre-equilibration at elevated temperature of 323 K and a slow transfer rate of 1 Å per 1 ns were needed to eliminate most of the discussed water defects. However, it was found also that despite the longer equilibration, the formation of stable hydrogen-bonded complexes between BBP and water molecules could lead to trapping of polar water molecules into the hydrophobic region of the bilayer. Figure 9 shows an example of MD umbrella sampling of BBP in a POPC bilayer demonstrating that single water molecules can enter a bilayer being included in the hydrogen-bonded associate with BBP. Similar examples of the trapping of excess water molecules surrounding the polar portion of asparagine and arginine have been reported recently [84,85,87]. This behavior is of potential interest in the context of the use of BBP as fluorescent probes, since this type of the incomplete dehydration at penetration inside the lipid bilayer may influence its emission signal.

4. CONCLUSIONS

The fluorescence behavior of 2,6-bis(1*H*-benzimidazol-2-yl)pyridine was investigated in aqueous sodium phosphate buffer solution at pH 8 at the absence and at the presence of a model membrane. Our study demonstrated that BBP is weakly fluorescent in water; however it becomes highly fluorescent when partitioned into LUV. Complementary use of experimental and computational data suggested that the fluorescence enhancement of BBP in the hydrophobic environment of the bilayer is due to the loss of water-induced quenching. We found that, upon the water-to-LUV transfer, the fluorescence enhancement depends strongly on lipid composition of LUVs, varying from 8.5-fold increase for anionic 25POPC/75POPG LUV to 62-fold increase for pure POPC LUV. Despite this fact, fluorescence quenching of membrane-bound BBP by Co^{2+} ions demonstrated a weak dependence on variation in zwitterionic-to-anionic lipid ratios of LUVs, indicating that, when partitioned into these LUVs, the excited fluorophore becomes almost completely shielded from the quencher. From LUV titration experiments we found that the Gibbs free energy (ΔG) of transfer of BBP from the bulk water inside the bilayer is strongly thermodynamically favored, depending only insignificantly upon a fraction of charged lipids in LUV. This indicates that partitioning is mainly driven by hydrophobic effects, when hydrophobic BBP tends to move from polar water surrounding into the apolar inner region of LUV. Our fluorescence experiments were supported by a series of atomistic MD simulations based on free redistributing BBP between the bulk water and a POPC bilayer. The equilibrium simulation showed that BBP binds rapidly and penetrates deeply into the hydrophobic region of the POPC bilayer. The constrained MD sampling of the penetration profile across the bilayer demonstrated that BBP favors residence in a broad region around 15 Å from the bilayer center, which is located between the hydrocarbon acyl tails and the initial portion of the lipid headgroups. It was also shown that the hydrophobic nature of this region of the bilayer restricts the permeability of water molecules, which may explain the strong enhancement of fluorescence properties of BBP when it occupies this area of the lipid bilayer.

Further progress in applying combinations of experimental fluorescence spectroscopy and the atomistic-level modeling to problems of the dye localization in a membrane may be augmented by new methodologies suitable for simulating spectral properties of a fluorophore in different environments using a hybrid quantum-classical *ab-initio*/MD approach. These studies are now underway in our laboratory, because developing of computational methods enabling prediction of a membrane partitioning behavior for new fluorescent probes prior to their synthesis can be a very promising tool to minimize the investment in probe design and development.

Supplementary Material

Refer to Web version on PubMed Central for supplementary material.

Acknowledgments

A.K, I.Yu.S, and A.O.D acknowledge support from Ukrainian Ministry of Education and Science grant M/83-2009. A.S.L acknowledges support from NIH grant GM-069783.

ABBREVIATIONS USED

BBP	2,6-bis(1*H*-benzimidazol-2-yl)pyridine
LUV	large unilamellar vesicles
POPC	1-palmitoyl-2-oleoyl-*sn*-glycero-3-phosphatidylcholine
POPG	1-palmitoyl-2-oleoyl-*sn*-glycero-3-phosphatidylglycerol
25POPC/75POPG and 75POPC/ 25POPG	mixtures of POPC and POPG that contain a molar percentage of the corresponding lipid specified by the number
Chol	cholesterol
90POPC/10Chol	a mixture that contain a molar percentage of 90:10 of POPC and cholesterol
MD simulation	molecular dynamics simulation
PMF	the potential of mean force

REREFENCES

1. Jurkiewicz P, Sýkora J, Olżyńska A, Humpolíčková J, Hof M. Solvent relaxation in phospholipid bilayers: Principles and recent applications. J. Fluorescence. 2005; 15:883–894.
2. Bagatolli LA. To see or not to see: Lateral organization of biological membranes and fluorescence microscopy. Biochim. Biophys. Acta. 2006; 1758:1541–1556. [PubMed: 16854370]
3. Demchenko AP, Mély Y, Duportail G, Klymchenko AS. Biophys. J. 2010; 96:3461–3470. [PubMed: 19413953]
4. Kachel K, Asuncion-Punzalan E, London E. The location of fluorescence probes with charged groups in model membranes. Biochim. Biophys. Acta. 1998; 1374:63–76. [PubMed: 9814853]
5. De Vequi-Suplicy CC, Benatti CR, Lamy MT. Laurdan in fluid bilayers: Position and structural sensitivity. J. Fluorescence. 2006; 16:431–439.

6. Asuncion-Punzalan E, London E. Control of the depth of molecules within membranes by polar groups: Determination of the location of anthracene-labeled probes in model membranes by parallax analysis of nitroxide-labeled phospholipid induced fluorescence quenching. Biochemistry. 1995; 34:11460–11466. [PubMed: 7547874]
7. Asuncion-Punzalan E, Kachel K, London E. Groups with polar characteristics can locate at both shallow and deep locations in membranes: The behavior of dansyl and related probes. Biochemistry. 1998; 37:4603–4611. [PubMed: 9521780]
8. Hoff B, Strandberg E, Ulrich AS, Tieleman DP, Posten C. ^{2}H-NMR study and molecular dynamics simulation of the location, alignment, and mobility of pyrene in bilayers. Biophys. J. 2005; 88:1818–1827. [PubMed: 15596514]
9. Loura LMS, Ramalho JPP. Location and dynamics of acyl chain NBD-labeled phosphatidylcholine (NBD-PC) in DPPC bilayers. A molecular dynamics and time-resolved fluorescence anisotropy study. Biochim. Biophys. Acta. 2007; 1768:467–478. [PubMed: 17141730]
10. Loura LMS, Fernandes F, Fernandes AC, Ramalho JPP. Effects of fluorescent probe NBD-PC on the structure, dynamics and phase transition of DPPC. A molecular dynamics and differential scanning calorimetry study. Biochim. Biophys. Acta. 2008; 1778:491–501. [PubMed: 18023411]
11. Hinner MJ, Marrink SJ, de Vries AH. Location, tilt, and binding: A molecular dynamics study of voltage-sensitive dyes in biomembranes. J. Phys. Chem. B. 2009; 113:15807–15819. [PubMed: 19894688]
12. Fraňová M, Repáková J, Čapková P, Holopainen JM, Vattulainen I. Effects of DPH on DPPC-cholesterol membranes with varying concentrations of cholesterol: From local perturbations to limitations in fluorescence anisotropy experiments. J. Phys. Chem. B. 2010; 114:2704–2711. [PubMed: 20136066]
13. Du B, Liu R, Zhang Y, Yang W, Sun W, Sun M, Peng J, Cao Y. Novel chemosensory materials based on polyfluorenes with 2-(2'-pyridyl)-benzimidazole and 5-methyl-3-(pyridin-2-yl)-1,2,4-triazole groups in the side chain. Polymer. 2007; 48:1245–1254.
14. Chetia B, Iyer PK. 2,6-Bis(2-benzimidazolyl)pyridine receptor for urea recognition. Tetrahedron Letters. 2006; 47:8115–8117.
15. Chetia B, Iyer PK. Utilization of 2,6-bis(2-benzimidazolyl)pyridine to detect toxic benzene metabolites. Tetrahedron Letters. 2007; 48:47–50.
16. Chetia B, Iyer PK. 2,6-Bis(2-benzimidazolyl)pyridine as a chemosensor for fluoride ions. Tetrahedron Letters. 2008; 49:94–97.
17. Aghatabay NM, Neshat A, Karabiyik T, Somer M, Haciu D, Dülger B. Synthesis, characterization and antimicrobial activity of Fe(II), Zn(II), Cd(II) and Hg(II) complexes with 2,6-bis(benzimidazol-2-yl) pyridine ligand. Europ. J. Med. Chem. 2007; 42:205–213.
18. Yu SC, Hou S, Chan WK. Synthesis, metal complex formation, and electronic properties of a novel conjugate polymer with a tridentate 2,6-bis(benzimidazol-2-yl)pyridine ligand. Macromolecules. 1999; 32:5251–5256.
19. Ayers T, Caylor N, Ayers G, Godwin C, Hathcock DJ, Stuman V, Slattery SJ. Design and investigation of a Ru(II) *N*-heterocyclic complex which undergoes proton coupled electron transfer. Inorganica Chimica Acta. 2002; 328:33–38.
20. Singh A, Chetia B, Mobin SM, Das G, Iyer PK, Mondal B. Ruthenium monoterpyridine complexes with 2,6-bis(benzimidazol-2-yl)pyridine: Synthesis, spectral properties and structure. Polyhedron. 2008; 27:1983–1988.
21. Vaidyanathan VG, Nair BU. Synthesis, characterization and DNA binding studies of a ruthenium(II) complex. J. Inorganic. Biochem. 2002; 91:405–412.
22. Wang J, Shuai L, Xiao X, Zeng Y, Li Z, Matsumura-Inoue T. Synthesis, characterization and DNA binding studies of a zinc complex with 2,6-bis(benzimidazol-2-yl) pyridine. J. Inorganic. Biochem. 2005; 99:883–885.
23. Mukherjee TK, Ahuja P, Koner AL, Datta A. ESPT of 2-(2′-pyridyl)benzimidazole at the micelle-water interface: Selective enhancement and slow dynamics with sodium dodecyl sulfate. J. Phys. Chem. A. 2005; 109:12567–12573.

24. Mukherjee TK, Panda D, Datta A. Excited-state proton transfer of 2-(2′-pyridyl)benzimidazole in microemulsions: Selective enhancement and slow dynamics in aerosol OT reverse micelles with an aqueous core. J. Phys. Chem. A. 2005; 109:18895–18901.
25. Kyrychenko A, Wu F, Thummel RP, Waluk J, Ladokhin AS. Partitioning and localization of environment-sensitive 2-(2'-pyridyl)- and 2-(2′-pyrimidyl)-indoles in lipid membranes: A joint refinement using fluorescence measurements and molecular dynamics simulations. J. Phys. Chem. B. 2010; 114:13574–13584. [PubMed: 20925327]
26. Kyrychenko A, Waluk J. Distribution and favorable binding sites of pyrroloquinoline and its analogues in a lipid bilayer studied by molecular dynamics simulations. Biophys. Chem. 2008; 136:128–135. [PubMed: 18556112]
27. Kyrychenko, A.; Waluk, J. Kinetics and Dynamics: from Nano- to Bio-Scale. In: Paneth, P.; Dybala-Defratyka, A., editors. Challenges and Advances in Computational Chemistry and Physics. Vol. 12. Springer Science+Business Media B.V.; New York: 2010. p. 35-75.
28. Addison AW, Burke PJ. Synthesis of some imidazole- and pyrazole- derived chelating agents. J. Heterocycl. Chem. 1981; 18:803–805.
29. Addison AW, Rao TN, Wahlgren CG. Synthesis of some benzimidazole- and benzothiazole-derived ligand systems and their precursory diacids. J. Heterocycl. Chem. 1983; 20:1481–1484.
30. Hope MJ, Bally MB, Mayer LD, Janoff AS, Cullis PR. Generation of multilamellar and unilamellar phospholipid vesicles. Chem. Phys. Lipids. 1986; 40:89–107.
31. Rodnin MV, Posokhov YO, Contino-Pépin C, Brettmann J, Kyrychenko A, Palchevskyy SS, Pucci B, Ladokhin AS. Interactions of fluorinated surfactants with diphtheria toxin T-domain: Testing new media for studies of membrane proteins. Biophys. J. 2008; 94:4348–4357. [PubMed: 18310255]
32. Bartlett GR. Phosphorus assay in column chromatography. J. Biol. Chem. 1959; 234:466–468. [PubMed: 13641241]
33. Melhuish WA. Quantum Efficiencies of fluorescence of organic substances: Effect of solvent and concentration of the fluorescent solute. J. Phys. Chem. 1961; 65:229–235.
34. Ladokhin AS, Jayasinghe S, White SH. How to measure and analyze tryptophan fluorescence in membranes properly, and why bother? Analytic. Biochem. 2000; 285:235–245.
35. Berger O, Edholm O, Jähnig F. Molecular dynamics simulations of a fluid bilayer of dipalmitoylphosphatidylcholine at full hydration, constant pressure, and constant temperature. Biophys. J. 1997; 72:2002–2013. [PubMed: 9129804]
36. Hermans J, Berendsen HJC, van Gunsteren WF, Postma JPM. A consistent empirical potential for water-protein interactions. Biopolymers. 1984; 23:1513–1518.
37. van der Spoel, D.; Lindahl, E.; Hess, B.; van Buuren, AR.; Apol, E.; Meulenhoff, PJ.; Tieleman, DP.; Sijbers, ALTM.; Feenstra, KA.; van Drunen, R.; Berendsen, HJC. Gromacs User Manual version 3.3. 2005. www.gromacs.org
38. Kyrychenko A, Stepanenko Y, Waluk J. Molecular dynamics and DFT studies of intermolecular hydrogen bonds between bifunctional heteroazaaromatic molecules and hydroxylic solvents. J. Phys. Chem. A. 2000; 104:9542–9555.
39. Berendsen HJC, Postma JPM, van Gunsteren WF, Dinola A, Haak JR. Molecular dynamics with coupling to an external bath. J. Chem. Phys. 1984; 81:3684–3690.
40. Darden T, York D, Pedersen L. Particle mesh Ewald: An $N\cdot\log(N)$ method for Ewald sums in large systems. J. Chem. Phys. 1993; 98:10089–10092.
41. Hees B, Bekker H, Berendsen HJC, Fraaije JGEM. LINCS: A linear constraint solver for molecular simulations. J. Comput. Chem. 1997; 18:1463–1472.
42. Kumar S, Bouzida D, Swendsen RH, Kollman PA, Rosenberg JM. The weighted histogram analysis method for free-energy calculations of biomolecules: I. The method. J. Comput. Chem. 1992; 13:1011–1021.
43. van der Spoel D, Lindahl E, Hess B, Groenhof G, Mark AE, Berendsen HJC. GROMACS: Fast, flexible and free. J. Comp. Chem. 2005; 26:1701–1718. [PubMed: 16211538]
44. Humphrey W, Dalke A, Schulten K. VMD: visual molecular dynamics. J. Mol. Graph. 1996; 14:33–38. [PubMed: 8744570]

45. Chou P-T. The host/guest type of excited-state proton transfer; a general review. J. Chin. Chem. Soc. 2001; 48:651–682.
46. López-Arbeloa T, López-Arbeloa F, Tapia MJ, López-Arbeloa I. Hydrogen-bonding effect on the photophysical properties of 7-aminocoumarin derivatives. J. Phys. Chem. 1993; 97:4704–4707.
47. Miyasaka H, Tabata A, Ojima S, Ikeda N, Mataga N. Femtosecond-picosecond laser photolysis studies on the mechanisms of fluorescence quenching induced by hydrogen-bonding interactions - 1-pyrenol-pyridine systems. J. Phys. Chem. 1993; 97:8222–8228.
48. Oshima J, Yoshihara T, Tobita S. Water-induced fluorescence quenching of mono- and dicyanoanilines. Chem. Phys. Lett. 2006; 423:306–311.
49. Wenska G, Koput J, Pedzinski T, Marciniak B, Karolczak J, Golankiewicz B. Effect of hydroxylic solvent on the fluorescence behavior of some bioactive 9-oxo-imidazo[1,2-a]purine derivatives. J. Phys. Chem. A. 2006; 110:11025–11033. [PubMed: 16986835]
50. Biczók L, Bérces T, Linschitz H. Quenching processes in hydrogen-bonded pairs: Interactions of excited fluorenone with alcohols and phenols. J. Am. Chem. Soc. 1997; 119:11071–11077.
51. Nosenko Y, Kunitski M, Thummel RP, Kyrychenko A, Herbich J, Waluk J, Riehn C, Brutschy B. Detection and structural characterization of clusters with ultrashort-lived electronically excited states: IR absorption detected by femtosecond. J. Am. Chem. Soc. 2006; 128:10000–10001. [PubMed: 16881614]
52. Nosenko Y, Kyrychenko A, Thummel RP, Waluk J, Brutschy B, Herbich J. Fluorescence quenching in cyclic hydrogen-bonded complexes of 1*H*-pyrrolo[3,2-*h*]quinoline with methanol: Cluster size effect. Phys. Chem. Chem. Phys. 2007; 9:3276–3285. [PubMed: 17579736]
53. Sobolewski AL, Domcke W, Dedonder-Lardeux C, Jouvet C. Excited-state hydrogen detachment and hydrogen transfer driven by repulsive $^1\pi\sigma^*$ states: A new paradigm for nonradiative decay in aromatic biomolecules. Phys. Chem. Chem. Phys. 2002; 4:1093–1100.
54. Sobolewski AL, Domcke W. Computational studies of the photophysics of hydrogen-bonded molecular systems. J. Phys. Chem. A. 2007; 111:11725–11735. [PubMed: 17941621]
55. Yu WS, Cheng CC, Cheng YM, Wu PC, Song YH, Chi Y, Chou PT. Excited-state intramolecular proton transfer in five-membered hydrogen-bonding systems: 2-Pyridyl pyrazoles. J. Am. Chem. Soc. 2003; 125:10800–10801. [PubMed: 12952455]
56. Kijak M, Zielińska A, Chamchoumis C, Herbich J, Thummel RP, Waluk J. Conformational equilibria and photoinduced tautomerization in 2-(2'-pyridyl)pyrrole. Chem. Phys. Lett. 2004; 400:279–285.
57. Kijak M, Nosenko Y, Singh A, Thummel RP, Waluk J. Mode-selective excited-state proton transfer in 2-(2'-pyridyl)pyrrole isolated in a supersonic jet. J. Am. Chem. Soc. 2007; 129:2738–2739. [PubMed: 17305339]
58. Chou PT, Wei CY, Chang CP, Meng-Shin K. Structure and thermodynamics of 7-azaindole hydrogen-bonded complexes. J. Phys. Chem. 1995; 99:11994–12000.
59. Vendrell O, Gelabert R, Moreno M, Lluch JM. Exploring the effects of intramolecular vibrational energy redistribution on the operation of the proton wire in green fluorescent protein. J. Phys. Chem. B. 2008; 112:13443–13452. [PubMed: 18826182]
60. Nosenko Y, Kunitski M, Riehn C, Thummel RP, Kyrychenko A, Herbich J, Waluk J, Brutschy B. Separation of different hydrogen-bonded clusters by femtosecond UV-ionization-detected infrared spectroscopy: 1*H*-pyrrolo[3,2-h] quinoline·$(H_2O)_n$=1,2 complexes. J. Phys. Chem. A. 2008; 112:1150–1156. [PubMed: 18215027]
61. Matsumoto Y, Ebata T, Mikami N. Structure and photoinduced excited state keto-enol tautomerization of 7-hydroxyquinoline-$(CH_3OH)_n$ clusters. J. Phys. Chem. A. 2002; 106:5591–5599.
62. Kohtani S, Tagami A, Nakagaki R. Excited-state proton transfer of 7-hydroxyquinoline in a non-polar medium: mechanism of triple proton transfer in the hydrogen-bonded system. Chem. Phys. Lett. 2000; 316:88–93.
63. Manca C, Tanner C, Leutwyler S. Excited state hydrogen atom transfer in ammonia-wire and water-wire clusters. Int. Rev. Phys. Chem. 2005; 24:457–488.

64. Meuwly M, Bach A, Leutwyler S. Grotthus-type and diffusive proton transfer in 7-hydroxyquinoline·$(NH_3)_n$ clusters. J. Am. Chem. Soc. 2001; 123:11446–11453. [PubMed: 11707122]
65. Herbich J, Hung CY, Thummel RP, Waluk J. Solvent controlled excited-state behavior: 2-(2′-pyridyl)indoles in alcohols. J. Am. Chem. Soc. 1996; 118:3508–3518.
66. Kyrychenko A, Herbich J, Wu F, Thummel RP, Waluk J. Solvent-induced *syn-anti* rotamerization of 2-(2′-pyridyl)indole and the structure of its alcohol complexes. J. Am. Chem. Soc. 2000; 122:2818–2827.
67. Kyrychenko A, Herbich J, Izydorzak M, Gil M, Dobkowski J, Wu FY, Thummel RP, Waluk J. Photoinduced double proton transfer: Inter- and intramolecular cases. Israel Journal of Chem. 1999; 39:309–318.
68. Kijak M, Petkova I, Toczek M, Wiosna-Sałyga G, Zielińska A, Herbich J, Thummel RP, Waluk J. Conformation-dependent photophysics of bifunctional hydrogen bond donor/acceptor molecules. Acta Phys. Polonica A. 2007; 112:S105–S120.
69. Petkova I, Mudadu MS, Singh A, Thummel RP, van Stokkum IHM, Buma WJ, Waluk J. Structure and photophysics of 2-(2′-pyridyl)benzindoles: The role of intermolecular hydrogen bonds. J. Phys. Chem. A. 2007; 111:11400–11409. [PubMed: 17935307]
70. Rode MF, Sobolewski AL. Photophysics of inter- and intra-molecularly hydrogen bonded systems: Computational studies on the pyrrole–pyridine complex and 2-(2′-pyridyl)pyrrole. Chem. Phys. 2008; 347:413–421.
71. Lan Z, Frutos LM, Sobolewski AL, Domcke W. Photochemistry of hydrogen-bonded aromatic pairs: Quantum dynamical calculations for the pyrrole–pyridine complex. Proc. Natl. Acad. Sci. USA. 2008; 105:12707–12712. [PubMed: 18663223]
72. Vetokhina V, Kijak M, Wiosna-Sałyga G, Thummel RP, Herbich J, Waluk J. On the origin of fluorescence quenching of pyridylindoles by hydroxylic solvents. Photochem. Photobiol. Sci. 2010; 9:923–930. [PubMed: 20445933]
73. Gutiérrez-Merino C, Bonini de Romanelli IC, Pietrasanta LI, Barrantes FJ. Preferential distribution of the fluorescent phospholipid probes NBD-phosphatidylcholine and rhodamine-phosphatidylethanolamine in the exofacial leaflet of acetylcholine receptor-rich membranes from Torpedo marmorata. Biochemistry. 1995; 34:4846–4855. [PubMed: 7718591]
74. Caputo GA, London E. Using a novel dual fluorescence quenching assay for measurement of tryptophan depth within lipid bilayers to determine hydrophobic α-helix locations within membranes. Biochemistry. 2003; 42:3265–3274. [PubMed: 12641458]
75. Repáková J, Čapková P, Holopainen JM, Vattulainen I. Distribution, orientation, and dynamics of DPH probes in DPPC bilayer. J. Phys. Chem. B. 2004; 108:13438–13448.
76. Vácha R, Siu SWI, Petrov M, Böckmann RA, Barucha-Kraszewska J, Jurkiewicz P, Hof M, Berkowitz Max L. Jungwirth P. Effects of alkali cations and halide anions on the DOPC lipid membrane. J. Phys. Chem. A. 2009; 113:7235–7243. [PubMed: 19290591]
77. Grossfield A, Woolf TB. Interaction of tryptophan analogs with POPC lipid bilayers investigated by molecular dynamics calculations. Langmuir. 2002; 18:198–210.
78. Norman KE, Nymeyer H. Indole localization in lipid membranes revealed by molecular simulation. Biophys. J. 2006; 91:2046–2054. [PubMed: 16815896]
79. Li C, Yi M, Hu J, Zhou H-X, Cross TA. Solid-state NMR and MD simulations of the antiviral drug amantadine solubilized in DMPC bilayers. Biophys. J. 2008; 94:1295–1302. [PubMed: 17890391]
80. Koubi L, Tarek M, Klein ML, Scharf D. Distribution of halothane in a dipalmitoylphosphatidylcholine bilayer from molecular dynamics calculations. Biophys. J. 2000; 78:800–811. [PubMed: 10653792]
81. Berkowitz ML, Bostick DL, Pandit S. Aqueous solutions next to phospholipid membrane surfaces: Insights from simulations. Chem. Rev. 2006; 106:1527–1539. [PubMed: 16608190]
82. Vácha R, Berkowitz ML, Jungwirth P. Molecular model of a cell plasma membrane with an asymmetric multicomponent composition: Water permeation and ion effects. Biophys. J. 2009; 96:4493–4501. [PubMed: 19486672]
83. Tieleman DP. Computer simulations of transport through membranes: Passive diffusion, pores, channels and transporters. Proc. Australian Physiol. Soc. 2006; 37:15–27.

84. MacCallum JL, Bennett W,FD, Tieleman DP. Partitioning of amino acid side chains into lipid bilayers: results from computer simulations and comparison to experiment. J. Gen. Physiol. 2007; 129:6206–6210.

85. MacCallum JL, Bennett W,FD, Tieleman DP. Distribution of amino acids in a lipid bilayer from computer simulations. Biophys. J. 2008; 94:3393–3404. [PubMed: 18212019]

86. Johansson ACV, Lindahl E. Titratable amino acid solvation in lipid membranes as a function of protonation state. J. Phys. Chem. B. 2009; 113:245–253. [PubMed: 19118487]

87. Li L, Vorobyov I, MacKerell AD Jr, Allen TW. Is arginine charged in a membrane? Biophys. J.: Biophys. Lett. 2007; 93:L11–L13.

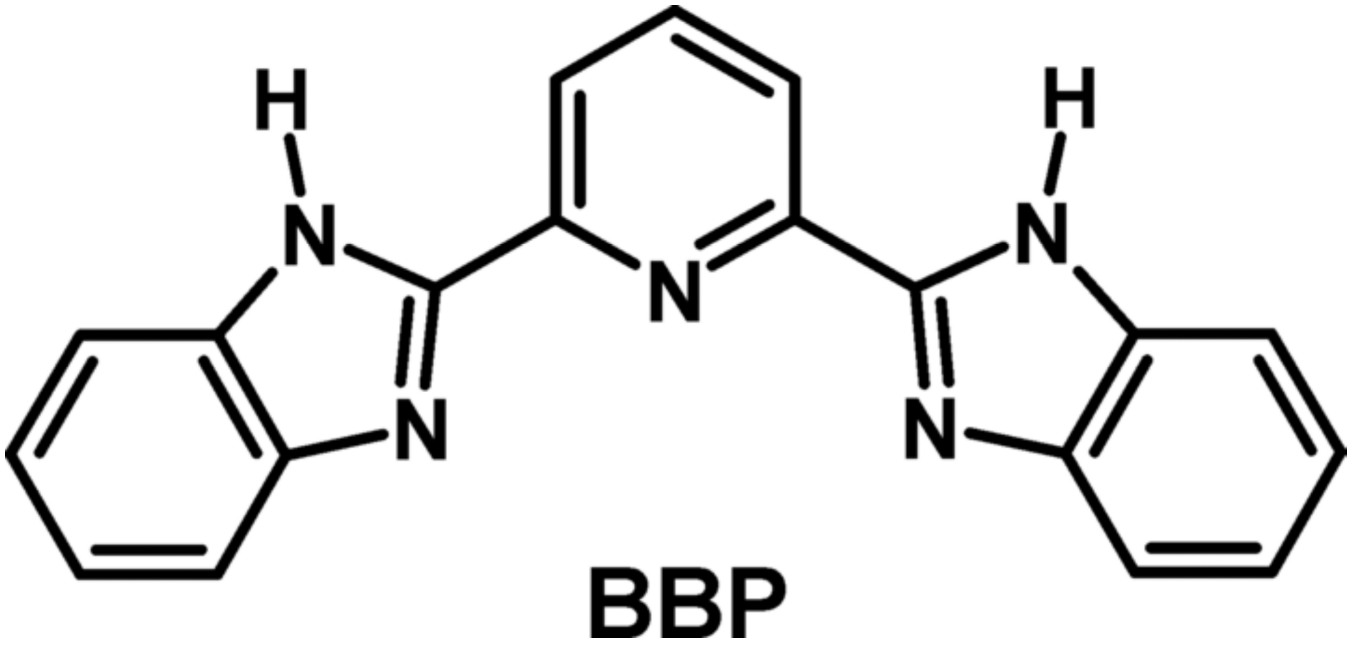

SCHEME 1.
Chemical structure of 2,6-bis(1*H*-benzimidazol-2-yl)pyridine (BBP).

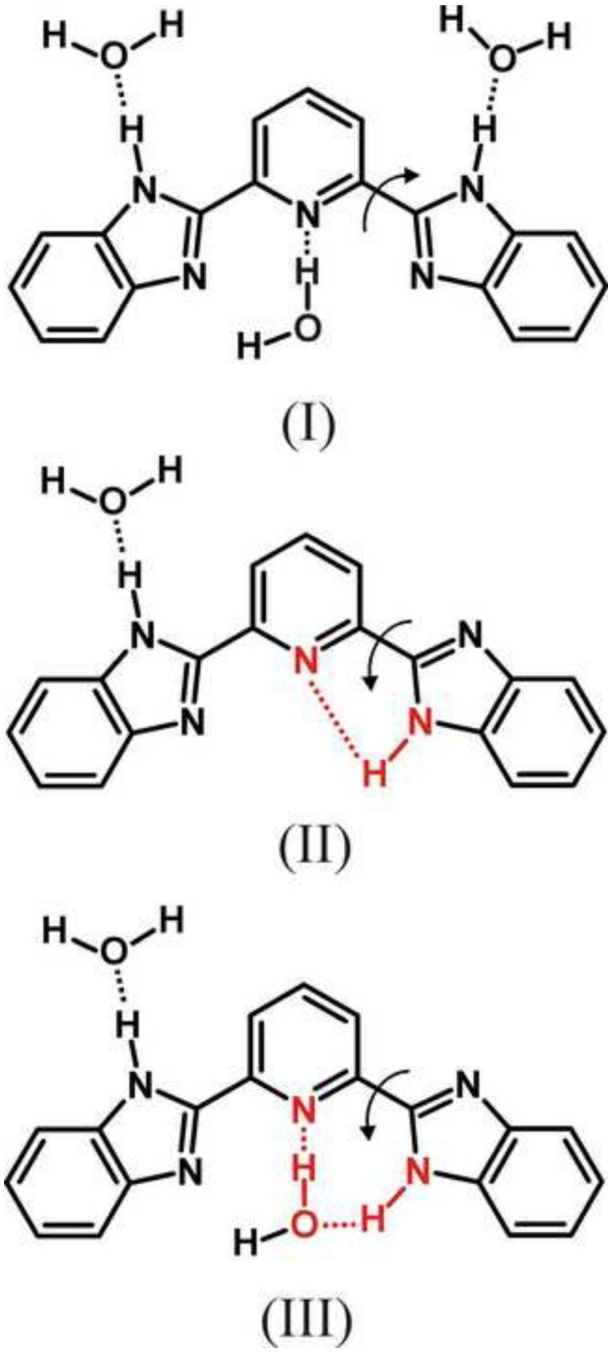

SCHEME 2.

Possible hydrogen-bonded forms of BBP: Form I shows a bifunctional hydrogen-bonding character of BBP, acting both as a donor and as an acceptor of a hydrogen bond. Forms II and III are capable of either direct intramolecular or solvent-assisted phototautomerization.

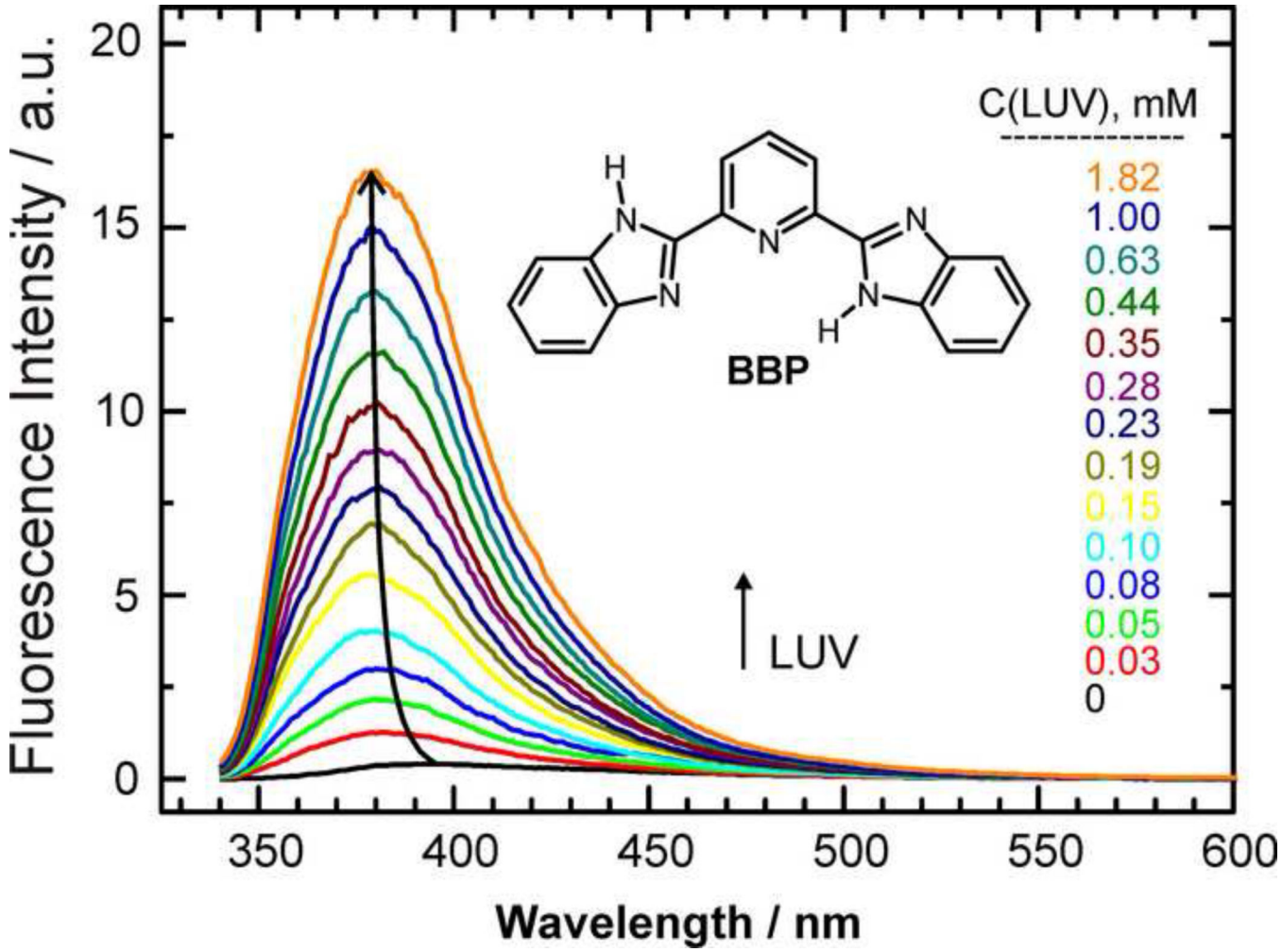

FIGURE 1.

Example of fluorescence titration of BBP upon adding POPC vesicles, measured in 50 mM sodium phosphate buffer at pH 8. An increase in the LUV concentration results in the strong fluorescence enhancement of BBP, which was also accompanied by a blue shift of its emission maximum. The arrows indicate the direction of changes at increasing LUV concentrations, varied in a range from 0 to 1.8 mM.

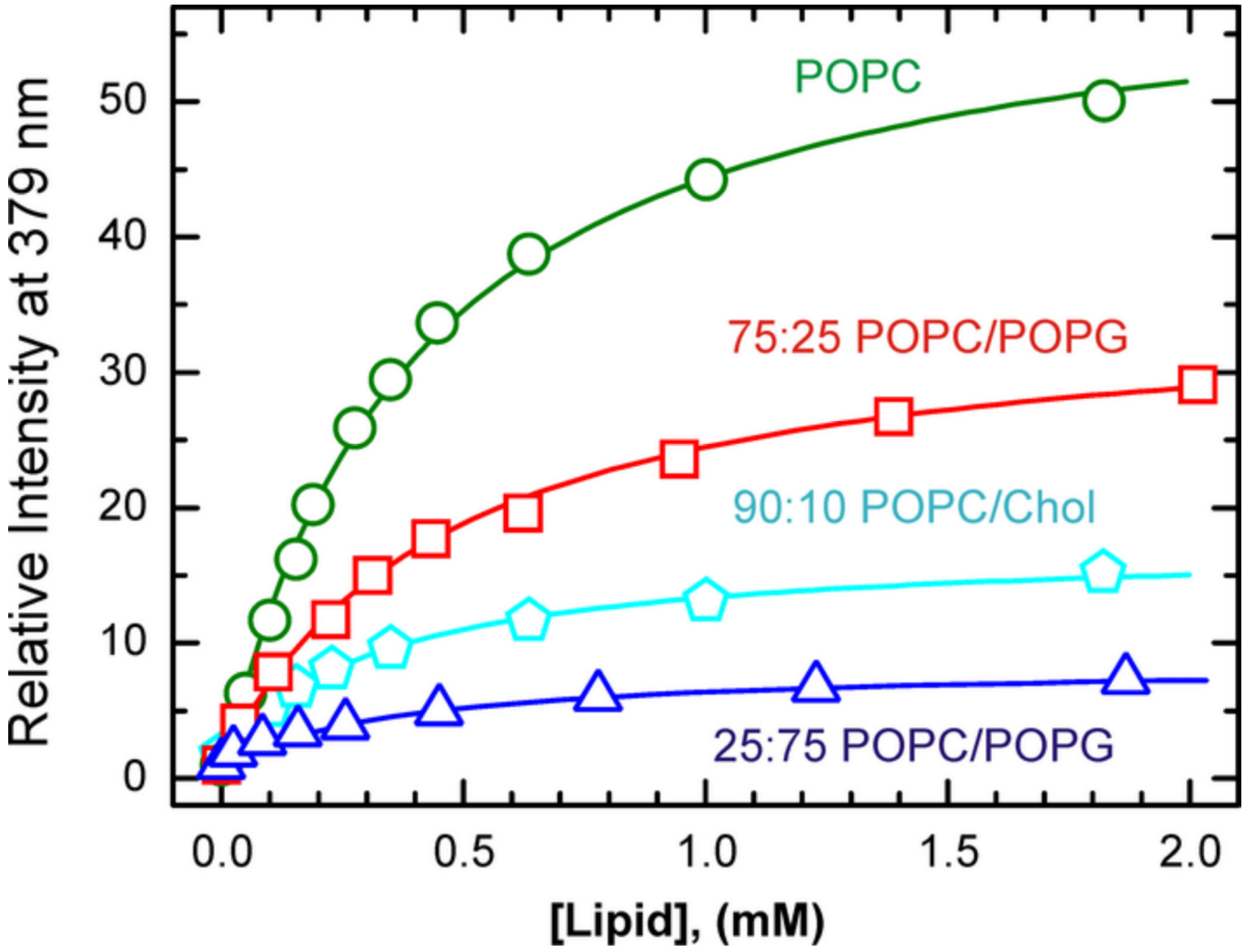

FIGURE 2.

Plots of the fluorescence enhancement of BBP observed upon LUV titration; POPC (green), 75POPC/25POPC (red), 90POPC/10Chol (cyan), and 25POPC/75POPG (blue). The titrations were performed in 50 mM sodium phosphate buffer at pH 8 at T=298 K. The relative fluorescence intensity at 379 nm was fitted to Eq. 1. Fitting results are shown with the colour-coded solid curves.

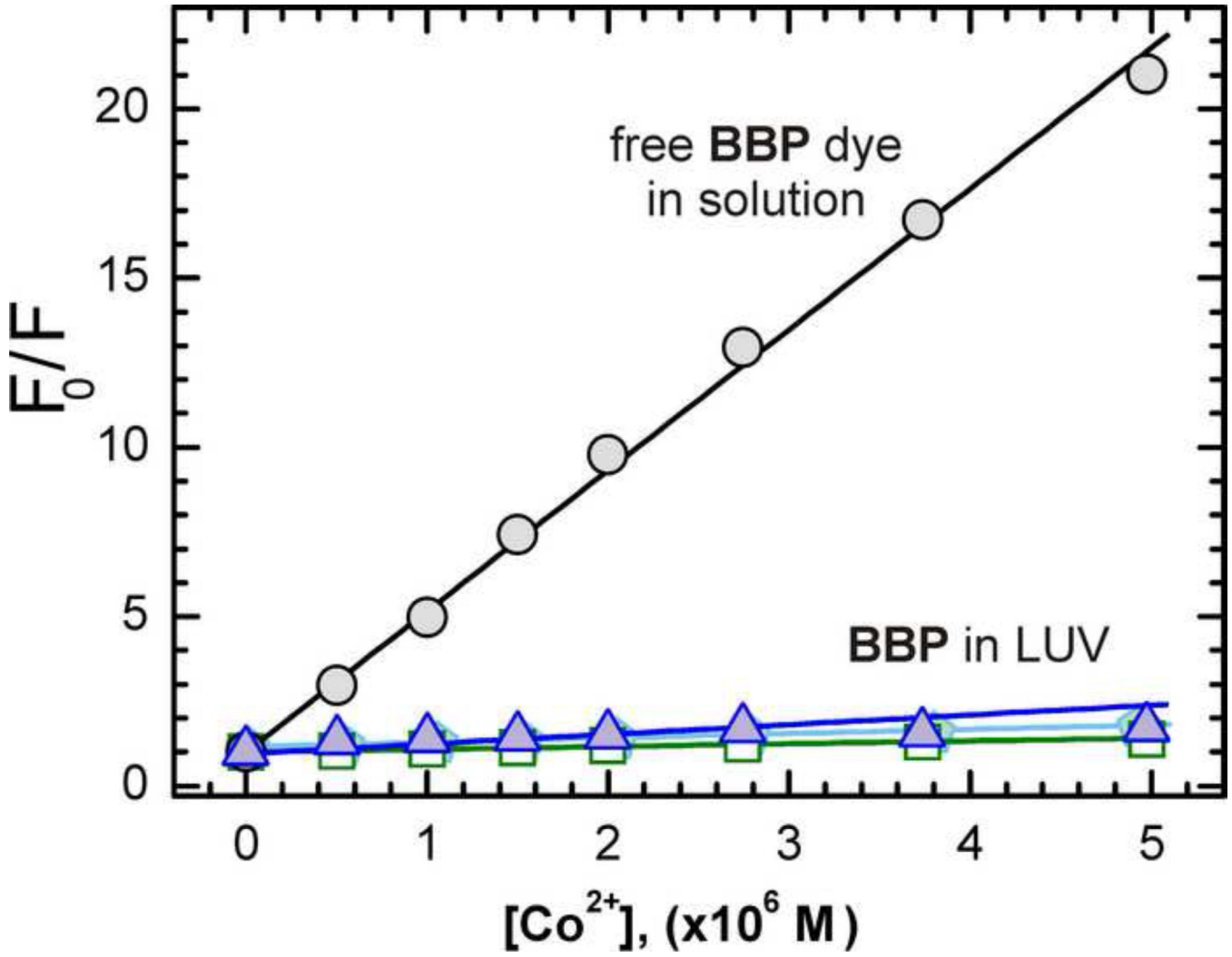

FIGURE 3.

Stern-Vollmer plots for BBP fluorescence quenching by Co^{2+} ions in sodium phosphate buffer at pH 8 in the absence and in the presence of lipid vesicles. The extent of fluorescence quenching of unbound BBP (○) changes strongly upon partitioning into LUVs (POPC (green □), 90POPC/10Chol (cyan ⬟), and 25POPC/75POPG (blue △)). The changes in quenching suggest that Co^{2+} ions do not readily penetrate the hydrophobic region of the lipid vesicle; so that the deeply buried BBP molecules become significantly inaccessible to the quencher. Fluorescence intensities were excited at 315 nm and measured at either 397 nm (free dyes) or 379 nm (in LUV). The quenching experiments in the presence of LUV were carried out at lipid saturation of 2 mM (see Figure 2 for more details).

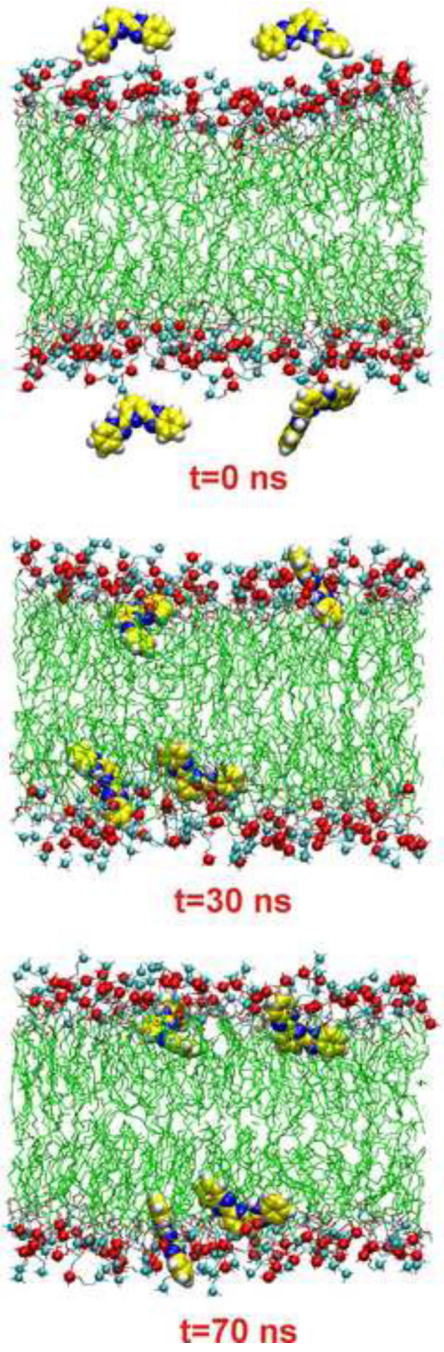

FIGURE 4.

Typical snapshots of MD simulations show the partitioning kinetics of BBP into a POPC bilayer at different simulation times. The MD simulations were based on free, passive distribution of probe molecules between bulk water and a POPC bilayer. Four probe molecules were sampled to ensure better MD statistics. The lipid tails are shown as sticks in green, the phosphorus and nitrogen atoms of the lipid headgroups are shown by red and cyan balls, respectively. For clarity, water molecules are not shown.

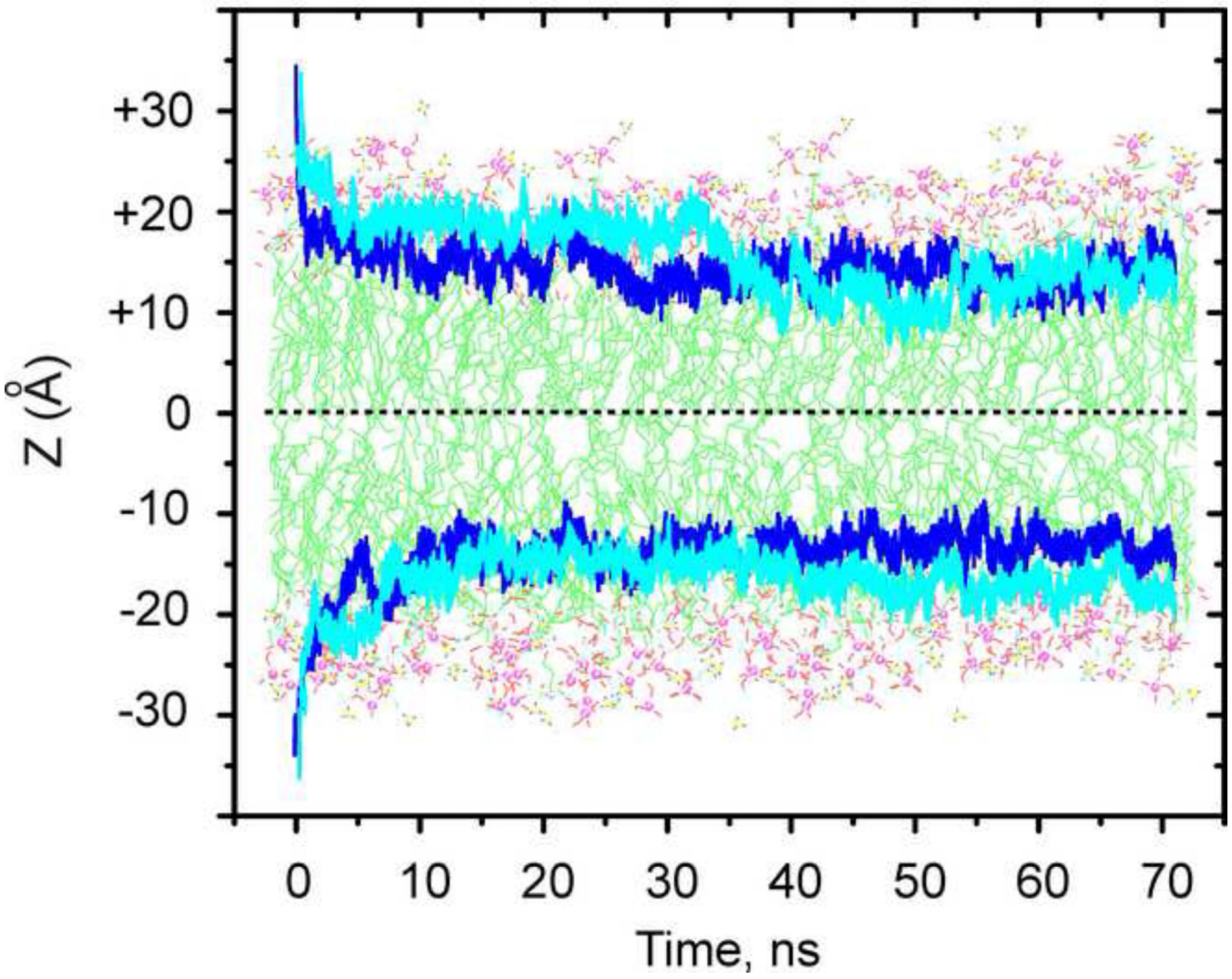

FIGURE 5.

MD trajectories of the partitioning kinetics of BBP into a POPC bilayer monitored by movements of the center-of-mass (COM) of each probe molecules with respect to the POPC bilayer normal *z*. The COM movements of the sampled molecules were traced to insure the complete equilibration and convergence of the MD system. The COM trajectories are schematically superimposed on a POPC snapshot.

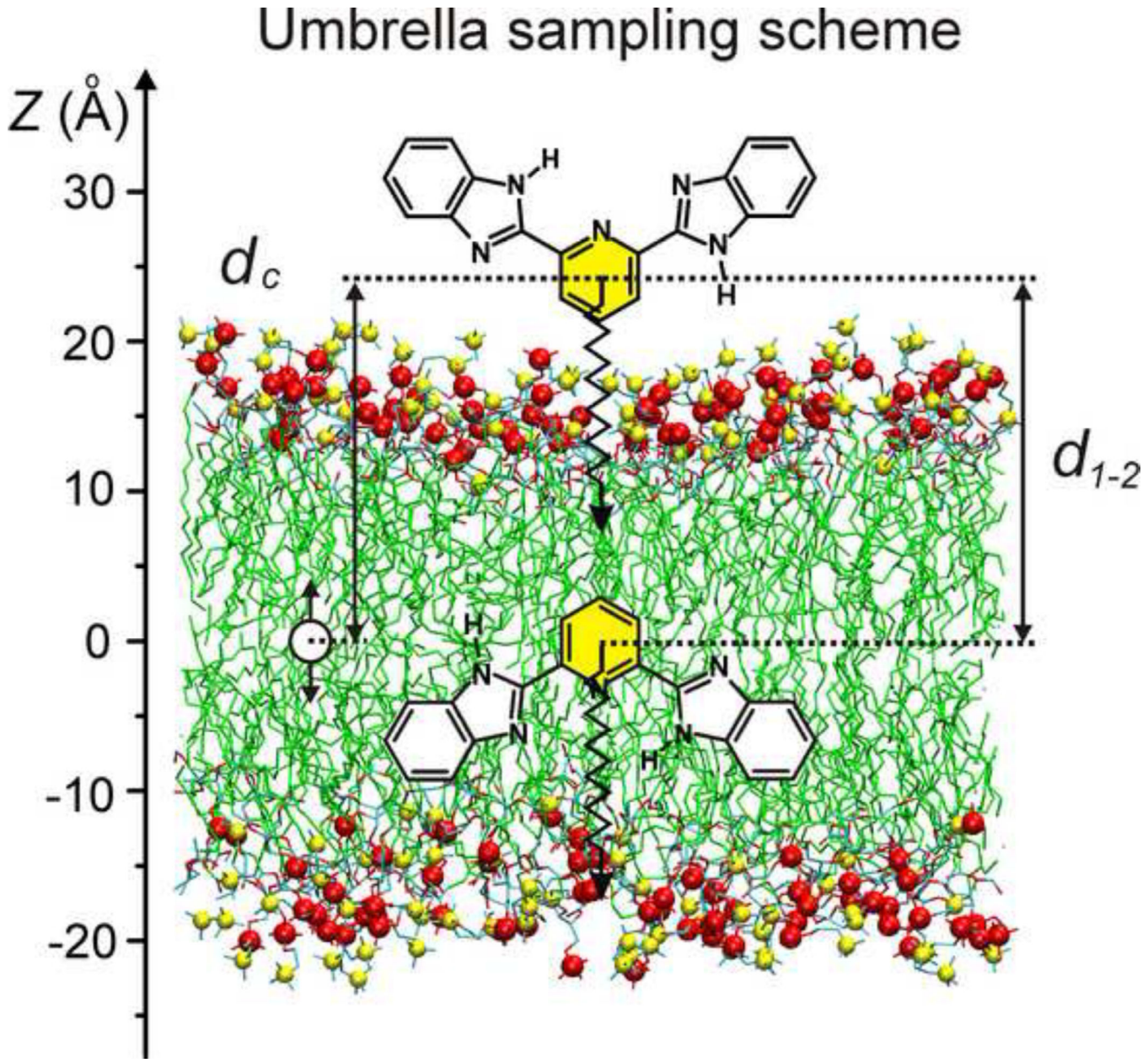

FIGURE 6.

A schematic presentation of the umbrella sampling scheme applied to evaluate a free energy profile for partitioning of BBP to a POPC bilayer. To gather additional MD sampling statistics, the two probe molecules were sampled simultaneously, so that when the first molecule was in the center of the bilayer, the second one was in bulk water. The harmonic restraint potential was applied to the distance d_c between the center of mass of the pyridine moiety (colored yellow) and the center of mass of the bilayer in direction Z normal to the bilayer. During the MD umbrella sampling, the two probe molecules were kept to be at the distance $d_{1\text{-}2}$ = 25 Å apart each other.

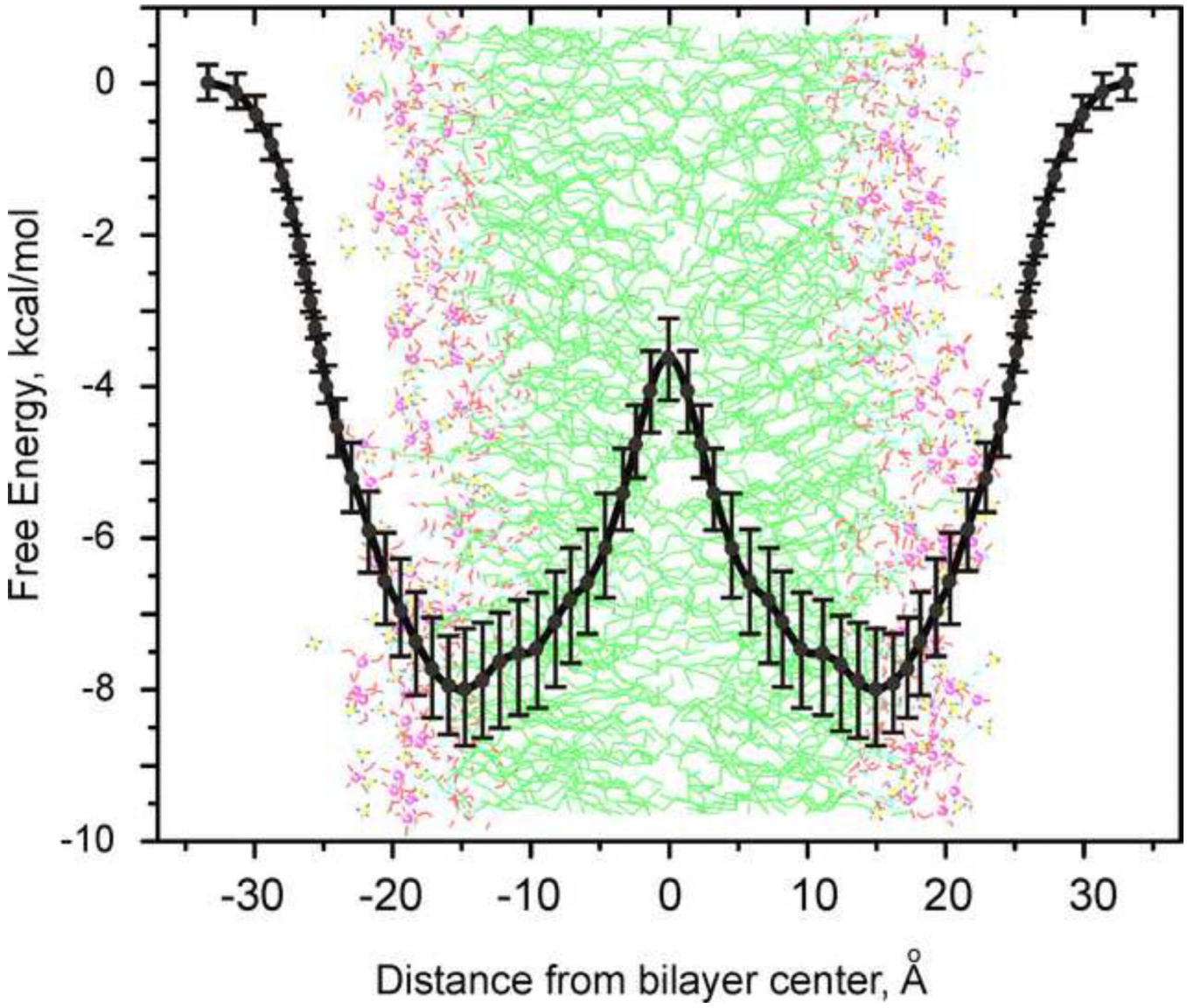

FIGURE 7.

MD simulations of a free energy profile of BBP penetration across a POPC bilayer calculated using the potential of mean constraint force. The PMF obtained according to the umbrella sampling scheme shown in Figure 6. The PMF was calculated from the biased distributions using the weighted histogram analysis method. The two BBP molecules were sampled simultaneously allowing for estimating sampling errors shown with corresponding error bars. The black solid line represents the average profile of the partitioning free energy. The partitioning profile is set to zero in bulk water. For the purpose of visualization, the PMF is schematically superimposed on a MD snapshot of a POPC bilayer.

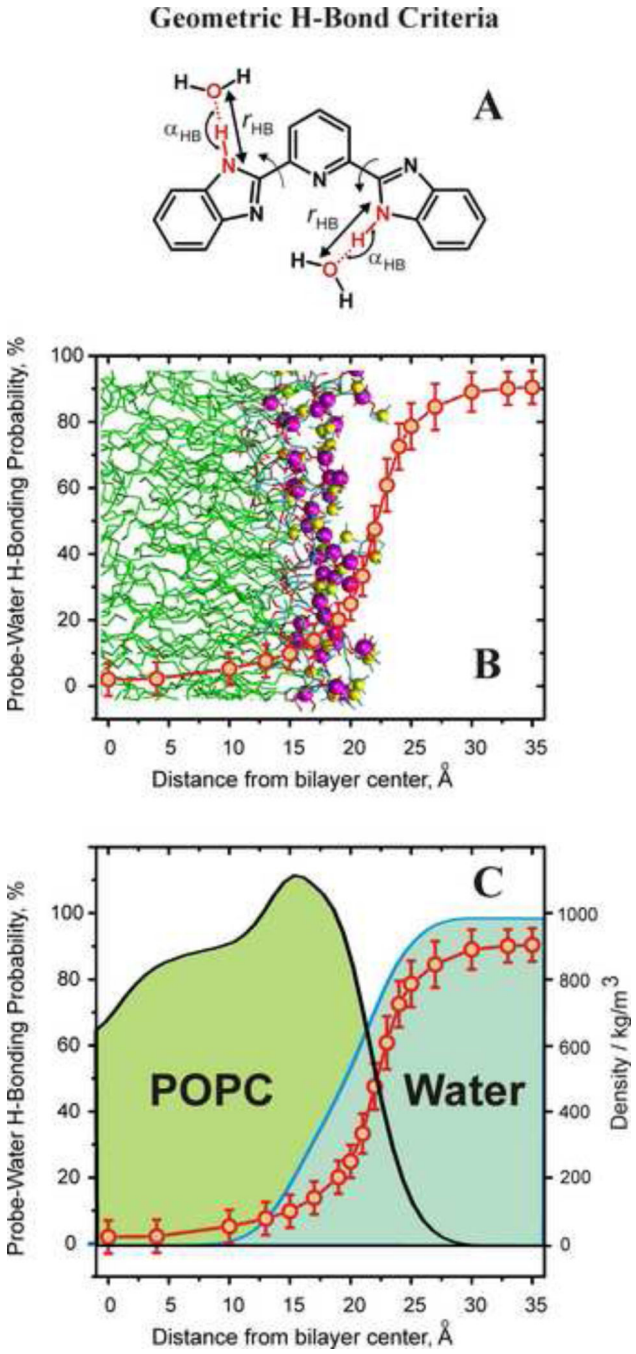

FIGURE 8.

(**A**) Geometric criteria for the formation of hydrogen bond between the benzimidazole N-H groups of BBP and water molecules. (**B**) The probability profile for hydrogen-bonding between BBP and water molecules estimated during MD umbrella sampling of a penetration depth of BBP across a POPC bilayer (see Figure 7 for more details). The probability of BBP–water H-bonding is schematically superimposed on a snapshot of a POPC bilayer. (**C**) The BBP–water H-bonding probability is now superimposed on mass density profiles of a

POPC bilayer (*filled green*) and water (*filled cyan*) showing that the profile of the probe −water H-bonding correlates with a profile of water permeability into a bilayer.

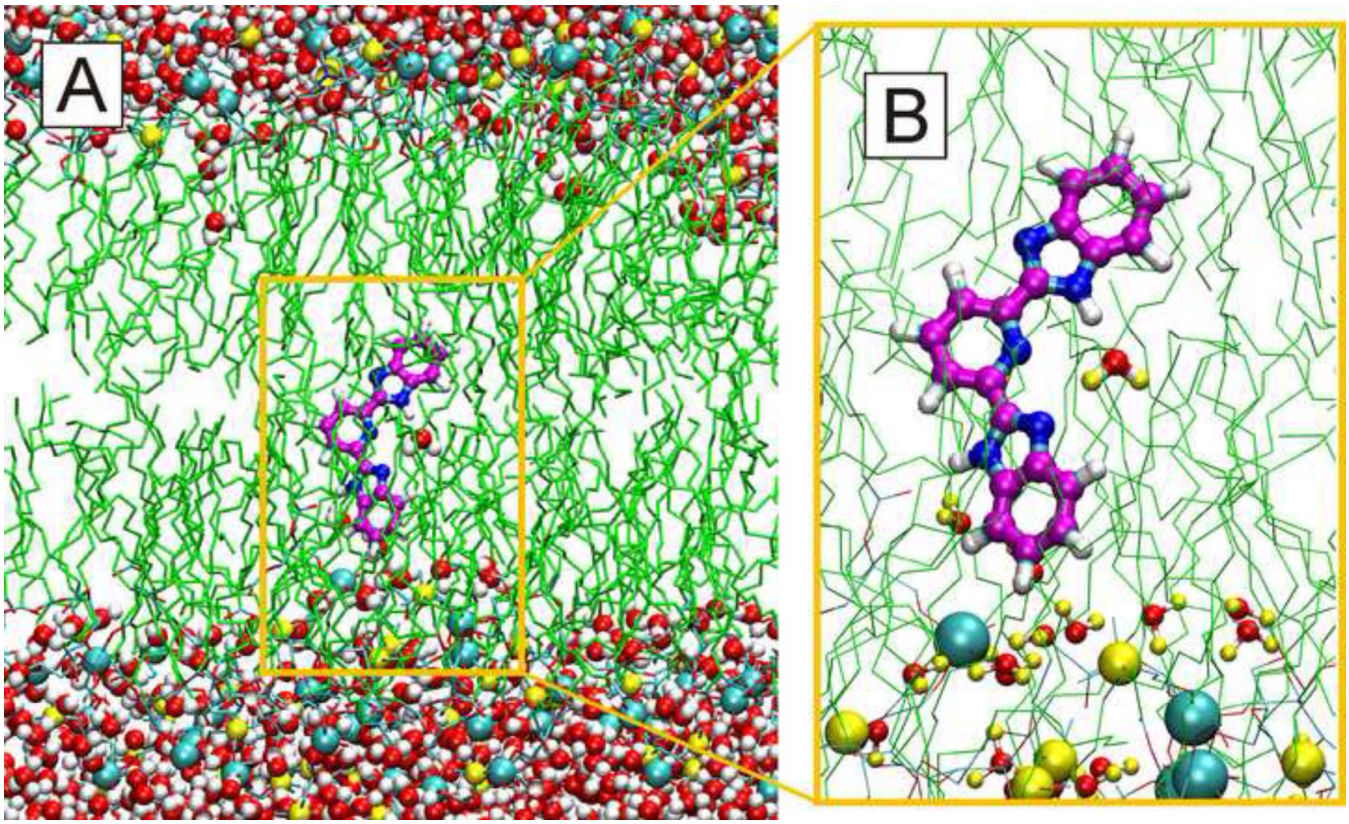

FIGURE 9.

Example of MD umbrella sampling of BBP in a POPC bilayer showing that excess water molecules can enter a bilayer in hydrogen-bonded associates with BBP. (**A**) The snapshot was obtained after 2 ns of MD umbrella sampling (see Figure 6 for more details), during which the pyridine ring of the fluorophore was constrained near the center of the bilayer. The lipid tails are green and the phosphorus and nitrogen atoms of the head groups of POPC are shown as cyan and yellow balls. (**B**) The insert demonstrates that the formation of a stable hydrogen-bonding complex between BBP and water molecules has led to the trapping of the water molecules into the hydrophobic core of the bilayer.

TABLE 1

Positions of maxima of electronic absorption spectra (λ_a), fluorescence spectra (λ_f), and fluorescence quantum yields (ϕ_{fl}) of BBP measured in organic solvents and in 50 mM sodium phosphate buffer at pH 8 in the absence and in the presence of 2 mM POPC vesicle.

Solvent	λ_a (nm)	λ_f (nm)	ϕ_{fl}
n-octane	334	367	0.22
toluene	333	370	0.37
ethyl acetate	328	374	0.46
acetonitrile	327	378	0.74
ethanol	338	375	0.48
sodium phosphate buffer at pH 8	342	395	0.005
in LUV (POPC)	339	379	0.31

TABLE 2 Parameters of the fluorescence enhancement and the thermodynamics of partitioning of BBP from aqueous buffer solution into a lipid vesicle.[a]

LUV composition	I_{max}	$K_p \times 10^{-4}$	ΔG, kcal/mol
POPC	61.7±0.3	15.4±1.1	−7.0±0.1
90POPC/10Chol	16.5±0.2	16.3±0.8	−7.1±0.1
75POPC/25POPG	33.8±0.2	14.1±1.2	−6.9±0.1
25POPC/75POPG	8.5±0.1	6.3±1.5	−6.5±0.1

[a]The maximal fluorescence increase on the complete partition (I_{max}), the molar partition coefficient (K_p), and the Gibbs free energy (ΔG) were measured in 50 mM sodium phosphate buffer at pH 8 at T=298 K.